Quantitative photoacoustic depth profilometry of magnetic field-induced thermal diffusivity inhomogeneity in the liquid crystal octylcyanobiphenyl

Andreas Mandelis[a)]
Photoacoustic and Photothermal Sciences Laboratory and Ontario Laser and Lightwave Research Center, Department of Mechanical Engineering, University of Toronto, Toronto M5S 1A4, Canada

Els Schoubs
Laboratorium voor Akoestiek en Warmtegeleiding, Department of Physics, Katholieke Universiteit Leuven, B-3001 Leuven, Belgium

Samuel B. Paralta
Photoacoustic and Photothermal Sciences Laboratory and Ontario Laser and Lightwave Research Center, Department of Mechanical Engineering, University of Toronto, Toronto M5S 1A4, Canada

Jan Thoen
Laboratorium voor Akoestiek en Warmtegeleiding, Department of Physics, Katholieke Universiteit Leuven, B-3001 Leuven, Belgium

(Received 8 February 1991; accepted for publication 2 May 1991)

An observed change in the photoacoustic signal frequency response upon the application of a transverse magnetic field across octylcyanobiphenyl samples in the nematic phase at 37 °C and 37.5 °C is reported. The application of a recent thermal-wave theory developed for depth profiling of continuously inhomogeneous condensed phases has given quantitative profiles of thermal diffusivity decreases extending to 20–30 μm below the liquid crystal surface. These decaying depth profiles are qualitatively consistent with earlier photoacoustic temperature scans of liquid crystals and are a measure of the extent of bulk reorientational effects due to the magnetic field, as well as the extent of the influence of the surface as a domain reorientation inhibitor in the kG range.

I. INTRODUCTION

Conventionally, the measurement of static and dynamic thermal quantities in liquid crystals has been an important venue for locating the different phases and phase transitions. High-resolution calorimetric measurements of the static quantities enthalpy and heat capacity have been carried out by adiabatic scanning calorimetry[1] or using ac calorimetric techniques.[2,3] On the other hand, thermal transport (dynamic) properties such as thermal conductivity have been studied using low-resolution steady-state gradient and transient techniques.[4–6] Very recently, photoacoustic spectroscopy (PAS) has proven to be capable of high-resolution measurements of the temperature dependence of several static and dynamic parameters in liquid crystals,[7–10] namely the thermal diffusivity, heat capacity, and thermal conductivity, especially across the region of phase transitions. As a result of the photoacoustic measurement of the thermal conductivity of nonylcyanobiphenyl (9CB),[11] octylcyanobiphenyl (8CB),[9] and heptycyanobiphenyl (7CB) (Ref. 10) with and without an applied transverse magnetic field, a large change was observed between the nematic phase values of that parameter at low modulation frequencies: in the presence of a magnetic field **B** on the order of 0.1–0.5 T parallel to the sample surface, the minimum value of thermal conductivity was found to be ~20% lower than that without a field in both 8CB and 9CB with a chopping frequency of 80 Hz. At higher chopping frequencies (~320 Hz) 9CB exhibited much smaller difference (~5%) in the conductivity values with and without an applied transverse magnetic field.[11] The opposite trends were evident in the values of the heat capacities, yet a difference is not expected between the $\mathbf{B}=\mathbf{0}$ and $\mathbf{B}>\mathbf{0}$ configurations for this parameter.[9] The above observations suggest that an inhomogeneous depth profile of the thermal conductivity may be present in these liquid crystals and the variation in the nematic value of the heat capacity may be an artifact, a consequence of using a photoacoustic formalism[12] for the data analysis based on the simple Rosencwaig–Gersho (RG) model,[13] which assumes constant (i.e., homogeneous) thermal parameters for the condensed phase sample.

In this work we performed detailed studies of the frequency dependence of the photoacoustic signal from 8CB in the nematic phase, in the presence and in the absence of an applied transverse magnetic field. Then we adapted a new thermal-wave model of continuously inhomogeneous condensed phases[14] to the photoacoustic detection scheme and solved the inverse problem, thus extracting quantitative depth profiles of the thermal diffusivity. These profiles were found to be in agreement with the above-mentioned trends in thermal conductivity and present, for the first time, a measure of the extent to which effects at the free-surface dominate bulk behavior in 8CB.

[a)]On leave at Laboratorium voor Akoestiek en Warmtegeleiding, Dept. of Physics, Katholieke University, Leuven, Belgium.

 0021-8979/91/031771-07$03.00

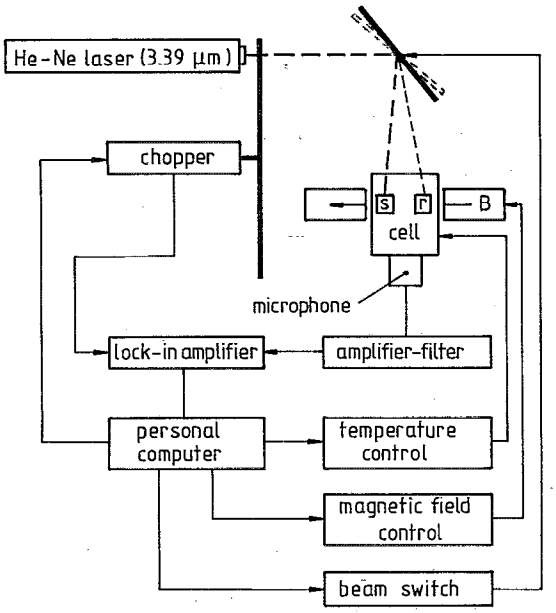

FIG. 1. Schematic diagram of the photoacoustic apparatus. *s* refers to the liquid crystal sample and *r* to the reference chamber. The arrow *B* gives the direction of the transverse magnetic field parallel to the sample surface.

II. EXPERIMENTAL AND RESULTS

A schematic diagram of the experimental apparatus is shown in Fig. 1. The actual PA cell is also shown in cross section in Fig. 2. For most of the frequency-domain PA measurements the 8CB sample itself without an applied magnetic field was the reference for the same sample response in the presence of a magnetic field. In a few cases pentylcyanobiphenyl (5CB), isotropic above 35 °C, was used as a reference sample for calibration of the frequency response of the PA cell. The sample was contained in a disklike slot of 8 mm diameter and 2.0 mm depth, machined in a removable gold-plated copper sample holder. A He-Ne laser operating at $\lambda = 3.39$ μm was chosen as the photoacoustic signal source, because this wavelength coincides with the strong absorption band of the C-H groups of the liquid crystal compounds. At 3.39 μm the optical absorption coefficient β of the 8CB has been reported to be[15] 6270 cm^{-1}, a value which would render the sample optically opaque and the PA signal at audio chopping frequencies would be expected to be independent of β, i.e., photoacoustically saturated.[13] This value of β may be somewhat too high. Other reports[8,10,11] used $\beta = 1600$ cm^{-1} for the optical absorption coefficient of 8CB. β was found to be constant as a function of temperature in each mesophase, with less than 3% deviation between the different phases. Even this value is probably too high. Fagard[16] used a β between 500 and 1000 cm^{-1}, resulting from fitting adjustments to the data. It thus appears that at 3.39 μm the liquid crystal 8CB may not be entirely photoacoustically saturated, even though the optical absorption depth β^{-1} is definitely shorter than the shortest thermal diffusion length considered in this work. Therefore, the calculated thermal diffusivity profile presented herein should be viewed as approximately correct, especially at reconstruction depths close to the sample surface. An exact treatment must take into account the extent of the optical absorption profile, as presented in Ref. 14, Eq. (37), and will be dealt with in a future publication.

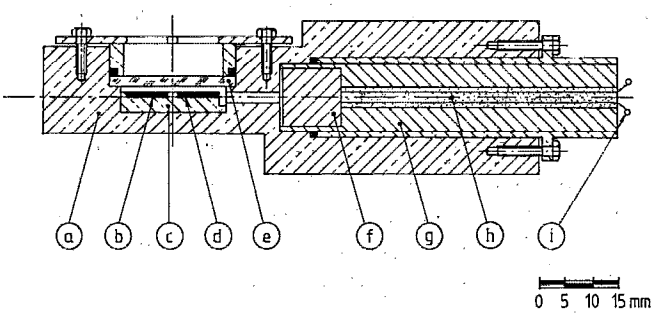

FIG. 2. Cross-sectional view of the PA cell. (a) Brass cell body, (b) liquid crystal sample, (c) sample holder, (d) reference chamber, (e) quartz window, (f) electret microphone, (g) microphone holder, (h) epoxy, (i) microphone leads to preamplifier.

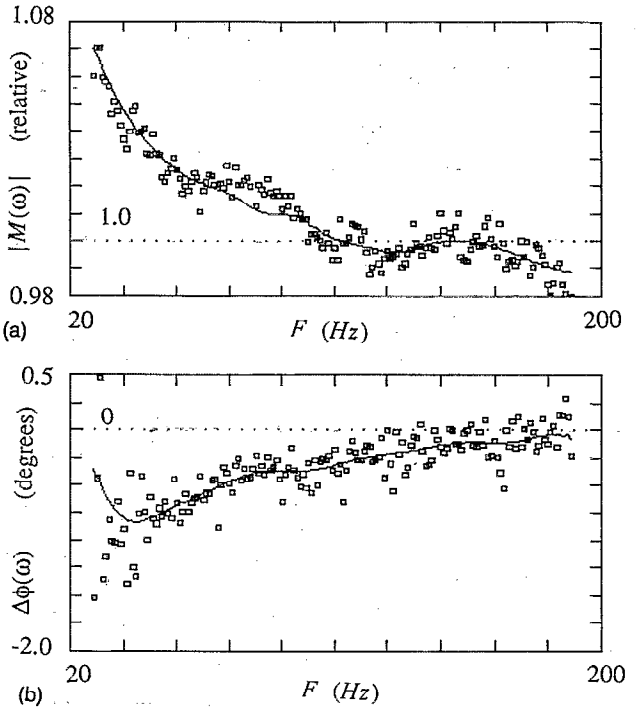

FIG. 3. (a) Amplitude ratio and (b) phase difference between an 8CB sample with an applied transverse magnetic field $B = 1.0$ kG, and the same sample with $B = 0$. The continuous lines drawn across the data are there to aid the eye and are the results of a smoothing technique.

Each experimental run in the presence of a transverse magnetic field was preceded by an identical run without the field and subsequently the PA signal amplitudes were ratioed and the phases were subtracted. The chopping frequency range chosen was between ~20 and 200 Hz. The lower limit was dictated by the requirement that the gas (air) column above the sample be thermally thick,[13] so as not to introduce signal behavior complications.[16] The up-

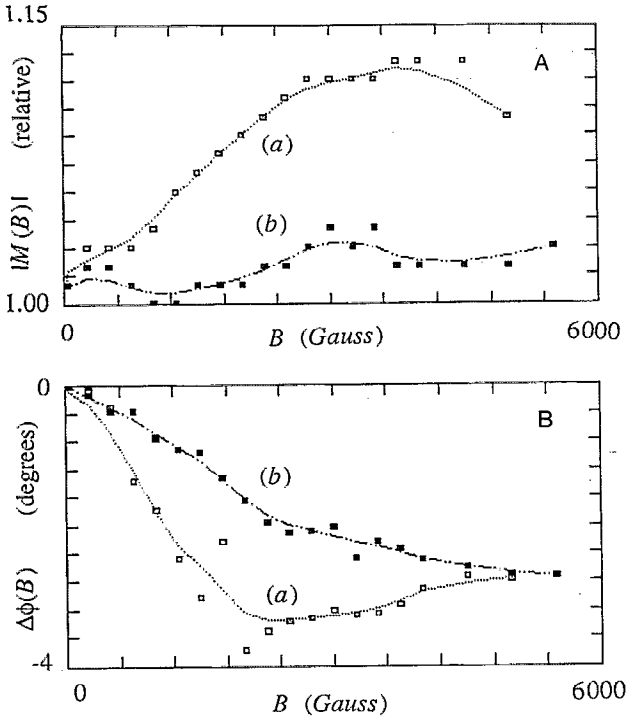

FIG. 4. (A) Amplitude ratio and (B) phase difference between an 8CB sample with an applied transverse magnetic field $B \lesssim 5$ kG and the same sample with $B = 0$. The lines connecting the data are there to aid the eye. Curves (a): 25 Hz; curves (b): 170 Hz.

per limit was determined by the virtual coincidence of both sample ($B > 0$) and reference ($B = 0$) signals.

The entire PA cell was temperature stabilized using temperature-sensing and electrical heating elements incorporated in the brass body of the cell.[8] An algorithm adjusted the heating power in a proportional integrated manner every 5 s. A personal computer controlled the temperature which was fixed at 37 or 37.5 °C, i.e., approximately in the middle of the nematic range of 8CB. The frequency scanning was done automatically by the computer, which controlled the mechanical chopper speed. Figure 3 shows typical amplitude ratios $|M(\omega)|$ and phase differences $\Delta\phi(\omega)$. The frequency increments were typically 1 or 2 Hz. The noise level was $\sim 2\%$ of the value of the PA amplitude and 0.5°–1° for the PA phase. Figure 4 shows the effect of the magnitude of an applied transverse magnetic field **B** on the PA amplitude and phase. It is seen that at low chopping frequencies, Fig. 4, curves (a), the signal amplitude increases with $|\mathbf{B}|$ and saturates for $|\mathbf{B}| \equiv B \gtrsim 3$ kG, whereas the phase still shows a slight variation above that value of the field magnitude. These trends are considerably less pronounced at high chopping frequencies, Fig. 4, curves (b). The observed increase in the PA amplitude and decrease in the phase lag with increased B are consistent with a decrease in the values of the dynamic thermal (transport) properties of the photoacoustically saturated 8CB sample upon application of a magnetic field. The fact that the high-frequency data show a much smaller variation indicates further that this thermal property change is essentially a bulk phenomenon, since the thermal diffusion length is shorter in that case and the PA probe essentially samples the near-the-surface region. This is entirely consistent with the trends in Fig. 3, which indicate that above ~ 100 Hz the $B > 0$ PA signals are similar to those with $B = 0$ and therefore surface effects dominate in that range, making the 8CB sample with $B > 0$ behave as it would with $B = 0$. This evidence is further corroborated by temperature measurements in the nematic region of 9CB and 7CB at low and high frequencies.[10,11]

III. NUMERICAL: THERMAL DIFFUSIVITY DEPTH PROFILING

The normalized thermal-wave temperature of a condensed phase sample with decreasing, continuously varying depth profiles of thermal parameters has been shown to be given by[14]

$$|M(\omega)|e^{i\Delta\phi(\omega)} = 1 + \tfrac{1}{4}R^{1/2}(\infty) \times \exp\left(-\frac{(1+i)\sqrt{\omega}}{2\sqrt{2}q}\frac{1}{\sqrt{\alpha_\infty}}\ln(\alpha_o/\alpha_\infty)\right) \quad (1)$$

for an optically opaque, thermally thick sample. In the above expression

$$R(\infty) \equiv e_s(0)/e_s(\infty), \quad (2)$$

where $e_s(x)$ is the depth-dependent thermal effusivity. The expression is valid for the decreasing thermal diffusivity depth profile

$$\alpha_s(x) = \alpha_o\left(\frac{1+\Delta e^{-qx}}{1+\Delta}\right)^2; \quad \Delta \equiv \left(\frac{\alpha_o}{\alpha_\infty}\right)^{1/2} - 1. \quad (3)$$

As was discussed in Ref. (14), arbitrary $\alpha_s(x)$ profiles can be handled by redefining the two constants (α_∞, q) at every chopping frequency $f_j = \omega_j/2\pi$ from the experimental data values, assuming knowledge of the surface value α_o.

When Eq. (1) is applied to the PA detection scheme, the adiabatic gas cell expression for the normalized pressure[13] simply becomes:

$$P(\omega) \equiv P_{\text{sample}}(\omega)/P_{\text{ref}}(\omega) = |M(\omega)|e^{i\Delta\phi(\omega)}, \quad (4)$$

where now $|M(\omega)|$ is the PA amplitude ratio and $\Delta\phi(\omega)$ is the PA phase difference. The form of Eq. (1) assumes that the value of the thermal diffusivity of the reference sample is α_o. Signal inversions yielding quantitative $\alpha_s(x)$ profiles can be produced from the experimental $|M(\omega)|$ and $\Delta\phi(\omega)$ data from neighboring chopping frequencies, such that[14]

$$\omega_{m-1} = \omega_m - \delta\omega; \quad \delta\omega \ll \omega_m, \quad (5)$$

by using

$$c_{m-1} = \left(\frac{2\sqrt{\omega_m}}{\delta\omega}\right)\ln\left(\frac{S(\omega_{m-1})}{S(\omega_m)}\right) \quad (6a)$$

$$= \frac{1}{2\sqrt{2}}\frac{\ln[\alpha_o/(\alpha_\infty)_{m-1}]}{q_{m-1}(\alpha_\infty)_{m-1}^{1/2}}, \quad (6b)$$

where

$$S^2(\omega_j) \equiv |M(\omega_j)|^2 + 1 - 2|M(\omega_j)|\cos[\Delta\phi(\omega_j)]. \quad (7)$$

Equation (6a) can now be used to determine c_{m-1}, i.e., the local value of c, from PA amplitude and phase data at frequencies f_m and f_{m-1}. Then, either the amplitude expression

$$|M(\omega_{m-1})|^2 = 1 + \tfrac{1}{2}R^{1/2}(\infty)e^{-c_{m-1}\sqrt{\omega_{m-1}}} \times \cos(c_{m-1}\sqrt{\omega_{m-1}}) + \tfrac{1}{16}R(\infty) \times e^{-2c_{m-1}\sqrt{\omega_{m-1}}} \quad (8a)$$

or the phase expression

$$\Delta\phi(\omega_{m-1}) = -\tan^{-1}\left(\frac{\tfrac{1}{4}R^{1/2}(\infty)e^{-c_{m-1}\sqrt{\omega_{m-1}}}\sin(c_{m-1}\sqrt{\omega_{m-1}})}{1+\tfrac{1}{4}R^{1/2}(\infty)e^{-c_{m-1}\sqrt{\omega_{m-1}}}\cos(c_{m-1}\sqrt{\omega_{m-1}})}\right), \quad (8b)$$

both directly obtainable from Eq. (1), may be used in order to locally determine the parameter $R(\infty)_{m-1}$. This parameter is related to α_∞ via:[14]

$$R(\infty)_{m-1} \approx \sqrt{\alpha_0/(\alpha_\infty)_{m-1}}. \quad (9)$$

Once $(\alpha_\infty)_{m-1}$ is calculated, Eq. (6b) can be used to evaluate locally at $\omega = \omega_{m-1}$ the q_{m-1} value.

Before inversion of actual PA data of the type shown in Fig. 3, smoothed frequency responses were obtained from the raw data, using a modification of a three-point averaging technique[17] found useful in previous work[18,19] for reducing the effect of random errors and improving the signal-to-noise ratio (SNR). A brief discussion of the importance and effect of data smoothing on the quality of the reconstructed $\alpha_s(x)$ profiles can be found in the Appendix. The modified three-point averaging technique consists of replacing each of the data points F_j by

$$F'_j = (F_{j-1} + WF_j + F_{j+1})/(2+W), \quad (10)$$

where the weighting factor W was introduced. As $W \to 0$, F'_j becomes a linearly interpolated point between F_{j-1} and F_{j+1}. Furthermore, as $W \to \infty$, F'_j converges toward F_j. A judicious choice of weighting for the data presented here was found to be $W=1$ or $W=2$. The continuous lines drawn through the data of Fig. 3 are the results of applying the described smoothing method. Similarly, Figs. 5(a) and 5(b) show the normalized PA frequency amplitude and phase response, respectively, from 8CB with $B = 1.65$ kG applied transversely with a permanent magnet at a temperature 37.5 °C. These data are the average of four in-frequency runs for $B=0$, and of ten runs with the applied transverse magnetic field. The smoothed curves were subsequently used to form the expressions Eqs. (6a) and (6b). Notice that

$$\left(\frac{\delta f}{f}\right)_{\min} \approx \frac{1\ \text{Hz}}{21\ \text{Hz}} = 0.048 \ll 1,$$

which justifies fully Condition (5). Once all pairs $[(\alpha_\infty)_j, q_j]$, $0 \leqslant j \leqslant j_{\max} = m$ were calculated, the thermal diffusivity profile $a_s(x_j)$ was found from Eq. (3) and is shown in Fig. 5c. The depth axis x_μ was calculated using[14]

$$x_{j-1} = \mu_{j-1} = \mu_j + \Delta\mu_{j-1}; \quad m > j > 0, \quad (11)$$

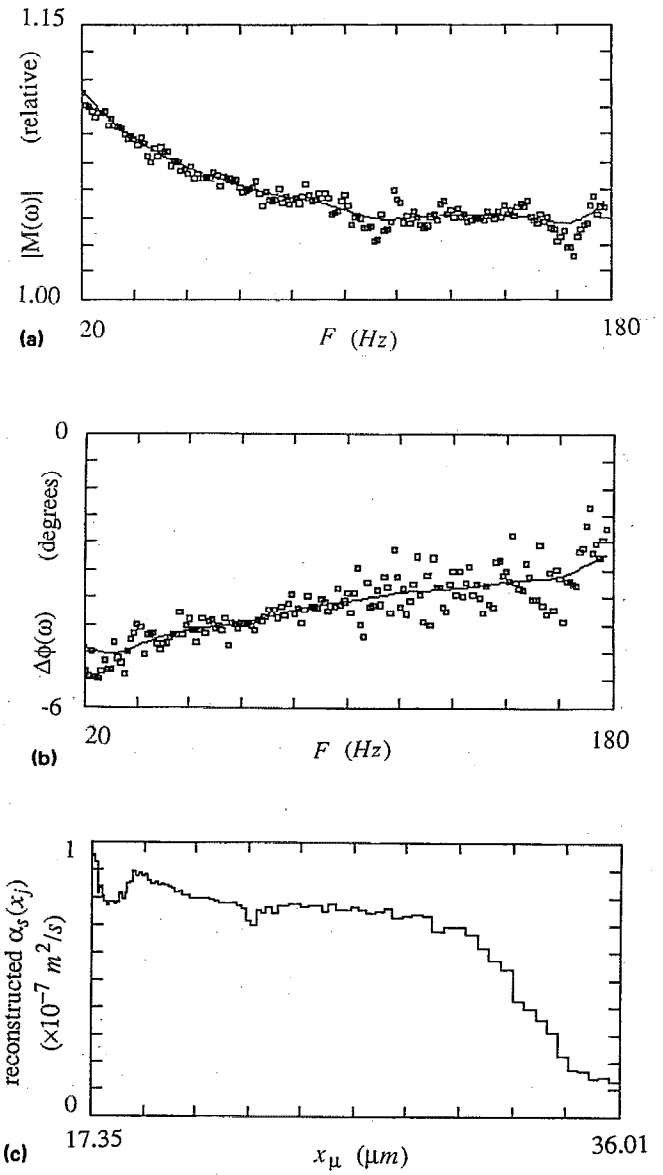

FIG. 5. (a) Amplitude ratio and (b) phase difference of averaged data between a nematic 8CB sample at 37.5 °C with an applied transverse magnetic field $B = 1.65$ kG, and the same sample with $B = 0$. The continuous lines are the smoothed data, (c) reconstructed thermal diffusivity profile.

where the thermal diffusion length at frequency f_m is

$$\mu_m=(2\alpha_o/\omega_m)^{1/2} \tag{12}$$

and with decreasing frequency $f_{j-1}<f_j$, an increase in the thermal diffusion length can be written as

$$\Delta\mu_{j-1}=(2\alpha_{j-1}/\omega_{j-1})^{1/2}-(2\alpha_{j-1}/\omega_j)^{1/2}. \tag{13}$$

As a surface thermal diffusivity value of the thinnest (surface) slice, applicable to the highest chopping frequency, f_m, data points, it was assumed that

$$\alpha_s(x;f_m)\approx\alpha_s(0)=\alpha_o=1\times10^{-7}\ \text{m}^2/\text{s}.$$

This value corresponds roughly[6] to the $\alpha_\parallel$ value for nematic 8CB at 37.5 °C, i.e., the thermal diffusivity along the director of the liquid crystal. A consequence of the scatter of the experimental data points at high chopping frequencies—which determine the near-the-surface portions of the diffusivity profiles—and the relatively degraded signal-to-noise ratio (SNR) at those frequencies—is that the reconstructed profile at shallow depths fluctuates rapidly exhibiting an artificial dip at ~18 μm [Fig. 5(c)] before recovering at depths of ~19–20 μm for our samples (see Appendix). The high reliability of values of $\alpha_s(x)$ at deeper layers is due to the high SNR at low frequencies, which determine the $\alpha_s(x)$ behavior at those depths. The reported thermal diffusivity profile in Fig. 5(c), therefore, includes only the more reliable region, while normalizing the initial value of the diffusivity at the shallowest depth to α_o. It is important to note that the reconstructed diffusivity profile remains essentially unaltered if, instead of Eqs. (1) and (3), one uses the $\alpha_s(x)$ expression appropriate for increasing $\alpha_s(x)$ profiles:[14]

$$\alpha_s(x)=\alpha_o\left(\frac{1-\Delta e^{-qx}}{1-\Delta}\right)^2;\quad \Delta\equiv1-\left(\frac{\alpha_o}{\alpha_\infty}\right)^{1/2}. \tag{14}$$

This insensitivity of the experimental $\alpha_s(x;f_j)$ reconstructed profile to the details of the assumed distribution $\alpha_s(x)$ is a result of the fact that the $\alpha_s(x;f_j)$ profile is entirely determined from local values $[(\alpha_\infty)_j,q_j]$ at each chopping frequency and thus the details of the assumed profile are only pertinent to two neighboring frequencies, say f_j and f_{j-1}. This is a major advantage of this reconstruction technique, as it is sensitive to the experimental data only.

IV. DISCUSSION

It is apparent from the thermal diffusivity profile that the application of a transverse magnetic field across the 8CB liquid crystal in the nematic phase generates a region in the bulk with lower thermal transport properties than near the surface. Figure 5(c) strongly indicates that "bulk" behavior commences at and below 26–28 μm from the surface, whereas a high diffusivity region, which presumably extends up to the surface itself, exists above that depth. It is also apparent that even at the highest chopping frequencies

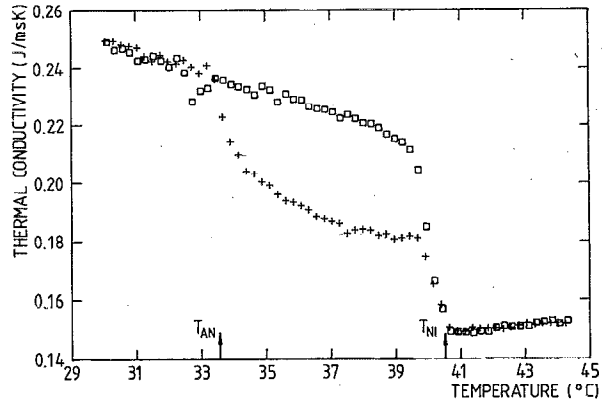

FIG. 6. Temperature dependence of the thermal conductivity of an 8CB sample from PA measurements at $f=80$ Hz. (□-□-□) data without a transverse magnetic field; (+ − + − +) data with a magnetic field $B\approx1$ kG in a direction parallel to the sample surface. T_{AN} and T_{NI} indicate the smectic A-to-nematic, and nematic-to-isotropic phase transition temperatures.

$$\mu_{\min}=\mu(180\ \text{Hz})$$
$$\approx13.3\ \mu\text{m}$$
$$>\beta^{-1}(3.39\ \mu\text{m})\approx1.6\text{–}10\ \mu\text{m},$$

i.e., the 2.00-mm thick 8CB sample is essentially optically opaque and thermally thick, thus at least approximately satisfying the assumptions behind Eqs. (1) and (8). From the definition of thermal diffusivity

$$\alpha_s(x)=k(x)/\rho(x)c(x) \tag{15}$$

and assuming that neither the liquid-crystal density $\rho(x)$ nor its specific heat $c(x)$ depend on the magnetic field,[9] then the profile reconstructed in this work is indicative of the depth variation of the thermal conductivity $k(x)$. Although this is the first time that such a variation is identified and described as a quantitative depth profile, yet it is consistent with the lowering of the nematic values of $k(T)$ in the presence of a transverse magnetic field in 8CB, when the conductivity is measured photoacoustically[9] at low chopping frequencies (Fig. 6). In terms of the liquid-crystal molecular orientation, the nematic phase has the translational symmetry of a fluid, but a broken rotational symmetry characterized by long-range orientational order, produced by the alignment of the long molecular axes along the director. In the nematic phase, however, the centers of mass of the molecules are still randomly distributed. Therefore, for the $B=0$ case one should normally expect an average thermal conductivity

$$\langle k\rangle=\tfrac{1}{3}(k_\parallel+2k_\perp) \tag{16}$$

for the uniaxial nematic mesophase,[20] with $k_\parallel$ and $k_\perp$ the conductivity values parallel and perpendicular, respectively, to the director in oriented samples. The large difference between the thermal conductivity in going from the isotropic phase to the nematic phase across T_{NI} in Fig. 6 is much larger than typically observed between $\langle k\rangle$ and k_{is} (the thermal conductivity for the isotropic phase) in the

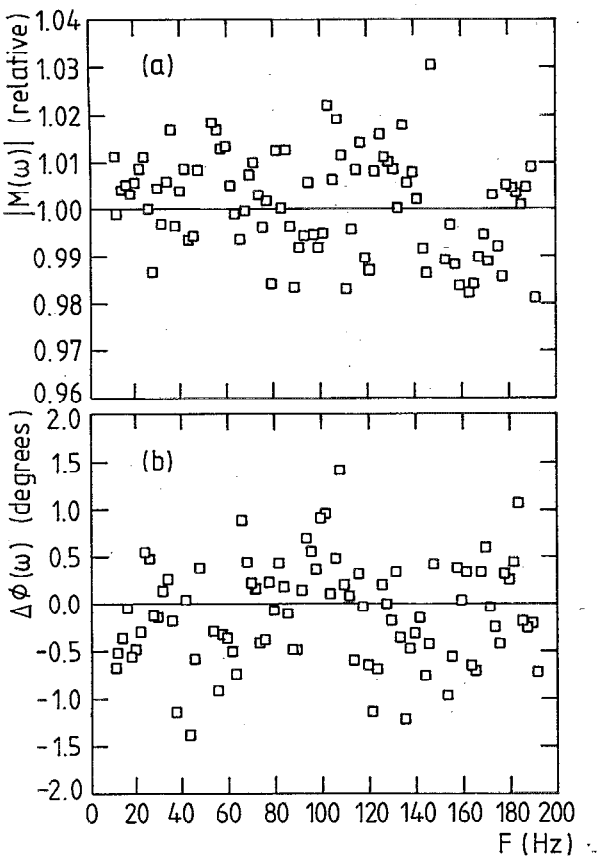

FIG. 7. (a) Amplitude ratio and (b) phase difference between an 8CB sample with an applied transverse magnetic field $B = 1.65$ kG, and the same sample with $B = 0$ in the isotropic phase (43 °C).

bulk of large size 8CB samples.[21] This fact suggests that in our sample $k_{\parallel}$ is dominant in the nematic phase, which may be the result of a surface-induced perpendicular alignment of the long molecular axes at the liquid-gas interface (i.e., the 8CB surface). Upon application of a transverse magnetic field, a realignment of some molecules along the **B** axis will increase the contribution of $k_{\perp}$ to the value of $\langle k \rangle$ and the value $\langle k \rangle = k_{\perp}$ would be expected for completely reoriented samples in strong **B** fields. Under these conditions, the mixture of $k_{\parallel}$ and $k_{\perp}$ contributions to $\langle k \rangle$ is expected to resemble the less anisotropic, more uniform distributions encountered in the isotropic phase, and indeed $\langle k(B>0) \rangle$ tends in that direction in Fig. 6, suggesting that $k_{\perp}$ is measurably and substantially smaller than $k_{\parallel}$. In the presence of relatively small magnetic fields ($\sim$1.65 kG), reorientation is apparently not complete and the effect of the surface as an orientation-pinning medium is dominant down to $\sim$26–28 μm. The trends in Fig. 4 suggest that bulk reorientational saturation occurs above $\sim$3 kG and thus substantially higher transverse magnetic fields may be required to overcome the surface-induced alignment of these rod-like molecules. Realignment seems more likely in the bulk, away from both gas-liquid and liquid-backing solid interfaces: the $L = 2.00$-mm thick samples used in this work were thermally thick ($\mu_{\max} \approx 51\ \mu\text{m} \ll L$), as well as geometrically thick, so as for the back interface not to have any measurable effect on the realignment of bulk molecules. For 300-μm thick 9CB samples in the nematic region it has also been found that realignment is not complete for a field close to 5 kG.[11] The presented depth profile is considered to be clear evidence that the interface-induced alignment perpendicular to the surface is a long-range phenomenon (tens of microns). This novel effect can be shown to be completely removed in the isotropic phase. Figure 7 shows PA amplitude ratios and phase differences with the setup identical to that which produced Fig. 5 and the 8CB crystal at 43 °C. Flat $\alpha_s(x)$ depth profiles result from these data, indicating the loss of anisotropy within the surface-dominated region. The present results may be significant for future studies of the long-range positional order of liquid crystal molecules due to interface-molecule interactions and of the effect of surfaces in phase transition behavior. This work also shows

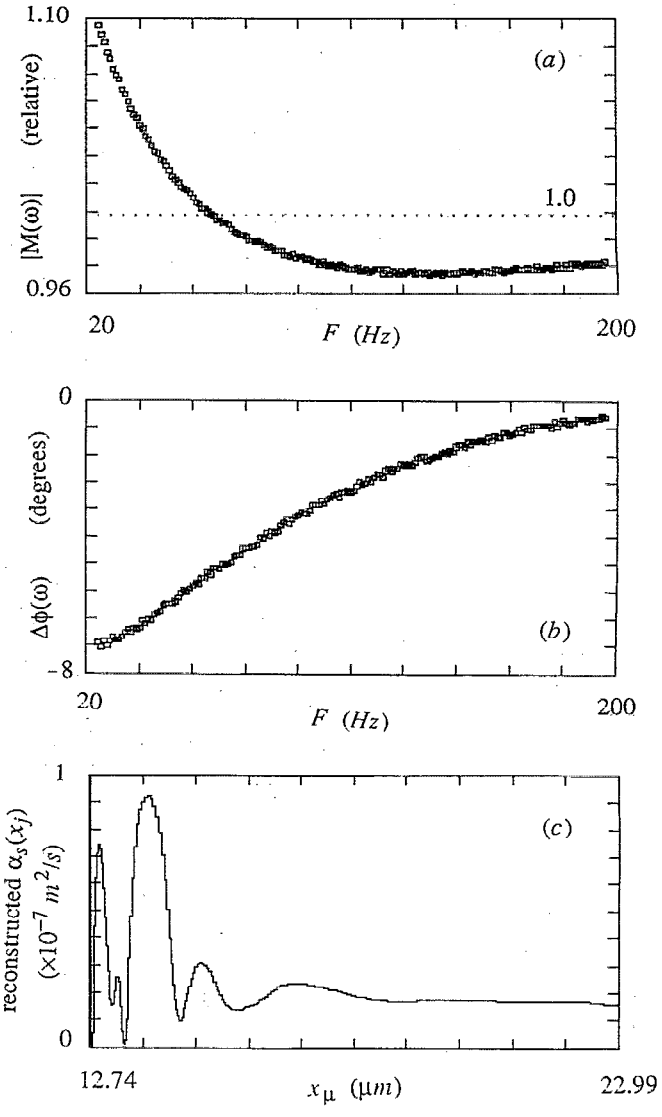

FIG. 8. (a) Simulated amplitude ratio and (b) phase difference of a PA signal with added random noise; (c) reconstructed thermal diffusivity. Random "noise" variables used: $\sigma_M = 0.1\%$, $\sigma_\phi = 0.1°$. (σ_M:amplitude noise; σ_ϕ: phase noise).

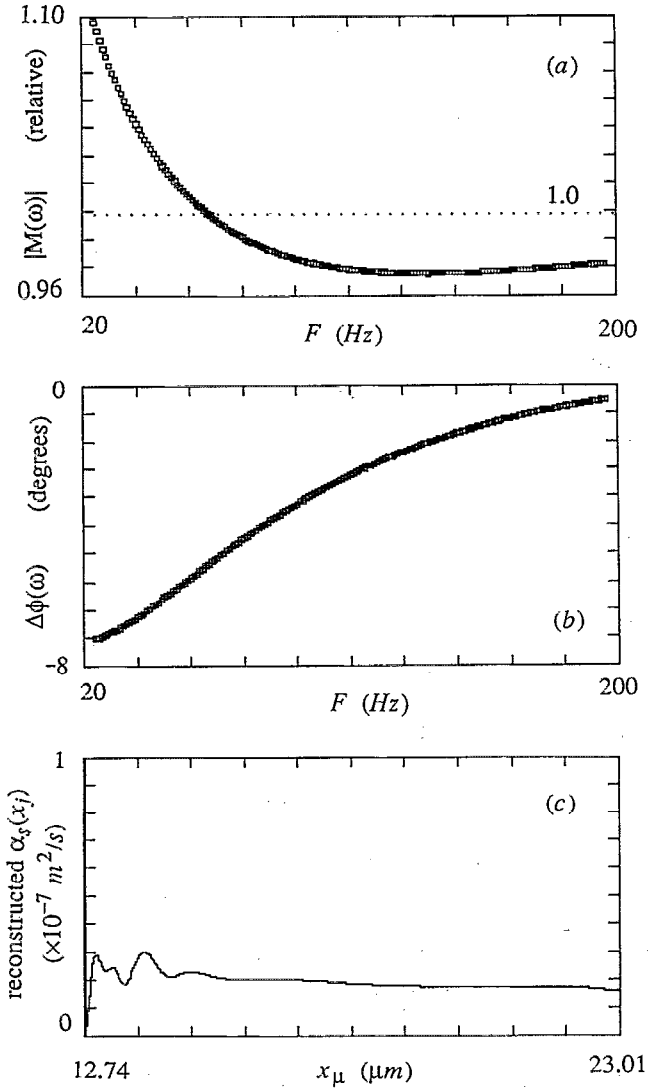

FIG. 9. Same as Fig. 8 except for the values of random "noise" variables added to the profile: $\sigma_M = 0.01\%$, $\sigma_\phi = 0.01°$.

the rich potential of PAS in the study of depth dependent thermophysical phenomena.

ACKNOWLEDGMENTS

We wish to gratefully acknowledge the support of the Natural Sciences and Engineering Research Council of Canada (NSERC), of the Ontario Laser and Lightwave Research Center (OLLRC), and of the Research Council of the Katholieke Universiteit Leuven.

APPENDIX: EFFECT OF RANDOM NOISE AND DATA SMOOTHING ON THERMAL DIFFUSIVITY RECONSTRUCTION METHOD

The need for smoothing of the raw data lies in the fact that our technique considers the sample to be composed of differential subsurface layers corresponding to a measurement at a modulation frequency $f_j = \omega_j/2\pi$. Since local $\alpha_s(x;f_j)$ values are determined, as discussed in Ref. 14 and in the text, by updating the values for the parameters c_j and $R(\infty)_j$ found at a neighboring frequency $f_{j+1} = \omega_{j+1}/2\pi$, random noise variations in the magnitude and phase from point to point can lead to fluctuations in the local estimate for the thermal diffusivity. This effect may be seen in Figs. 8 and 9, where simulated random errors have been introduced into otherwise smooth (simulated) magnitude and phase functions, with

$$\alpha_o = 1\times 10^{-7}\ \mathrm{m^2/s},\quad \alpha_\infty = 1\times 10^{-8}\ \mathrm{m^2/s},$$
$$q = 1\times 10^{5}\ \mathrm{m^{-1}}$$

in Eq. (3). An interesting observation is that, despite the rapid fluctuations at shallow depths (higher modulation frequencies), the reconstructed thermal diffusivity profile is self-correcting, becoming relative smooth at greater depths (lower modulation frequencies). If the random error introduced is lowered, as in Fig. 9, the fidelity of the reconstruction increases, and recovery from the fluctuation occurs much faster. An alternative to using such smoothing techniques, of course, is for experimental apparatus to be improved so as to operate more sensitively and with better SNR at high modulation frequencies, where the effect of fluctuations is greater.

The quantities c and $R(\infty)$ in this work are thus calculated at each frequency f_j from the smoothed magnitude and phase PAS data, assuming in our case $\alpha_o = 1\times 10^{-7}$ m^2/s, as determined for nematic liquid crystals. The thermal diffusivity spectrum $\alpha(f_j)$, and subsequently the depth profile $\alpha(x_j)$ are then calculated from these parameters, and used in the subsequent calculation at $f_{j-1} < f_j$ until the entire profile is reconstructed.

[1] J. Thoen, Phys. Rev. A **37**, 1754 (1988).
[2] K. J. Stine and C. W. Garland, Phys. Rev. A **39**, 3148 (1989).
[3] C. C. Huang, G. Nounesis, R. Geer, J. W. Goodby, and D. Guillon, Phys. Rev. A **39**, 3741 (1989).
[4] V. S. V. Rajan and J. J. C. Picot, Mol. Cryst. Liq. Cryst. **20**, 55 (1973).
[5] R. Vilanove, E. Guyon, C. Mitescu, and P. Pieranski, J. Phys. (Paris) **35**, 153 (1974).
[6] T. Akahane, M. Kondoh, K. Hashimoto, and M. Nagakawa, Jpn. J. Appl. Phys. **26**, L1000 (1987).
[7] M. Marinelli, U. Zammit, F. Scudieri, and S. Martellucci, Nuovo Cimento **9D**, 855 (1987).
[8] C. Glorieux, E. Schoubs, and J. Thoen, Mater. Sci. Eng. A **122**, 87 (1989).
[9] J. Thoen, E. Schoubs, and V. Fagard, Proc. Symp. Phys. Acoustics, Kortrijk Belgium (1990).
[10] J. Thoen, C. Glorieux, E. Schoubs, and W. Lauriks, Mol. Cryst. Liq. Cryst. **191**, 29 (1990).
[11] C. Glorieux, E. Schoubs, and J. Thoen, in *Photoacoustic and Photothermal Phenomena II*, edited by J. C. Murphy, J. W. Maclachlan-Spicer, L. C. Aamodt, and B. S. H. Royce (Springer, Berlin, 1990), p. 297.
[12] M. Marinelli, U. Zammit, F. Scudieri, S. Martellucci, J. Quartieri, F. Bloisi, and L. Vicari, Nuovo Cimento **9D**, 557 (1987).
[13] A. Rosencwaig and A. Gersho, J. Appl. Phys. **47**, 64 (1976).
[14] A. Mandelis, S. Peralta, and J. Thoen, J. Appl. Phys. **70**, 1761 (1991).
[15] G. Louis, P. Peretti, J. Billard, and B. Mangeot, Can. J. Phys. **64**, 1230 (1986).
[16] V. Fagard, Licentiaatsthesis, Katholieke Univ. Leuven, 1990, Chap. V.
[17] D. D. McCracken and W. S. Dorn, *Numerical Methods and FORTRAN Programming* (Wiley, New York, 1964).
[18] A. Mandelis, R. E. Wagner, K. Ghandi, R. Baltman, and P. Dao, Phys. Rev. B **39**, 5254 (1989).
[19] T. Dioszeghy and A. Mandelis, J. Phys. Chem. Solids **47**, 1115 (1986).
[20] P. G. de Gennes, *The Physics of Liquid Crystals* (Clarendon, Oxford, 1974).
[21] W. Urbach, H. Hervet, and F. Rondelez, Mol. Cryst. Liq. Cryst. **46**, 209 (1978).